LAWRENCE
LIVERMORE
NATIONAL
LABORATORY

UCRL-JRNL-222189

Edge Stability and Transport Control with Resonant Magnetic Perturbations in Collisionless Tokamak Plasmas

T. E. Evans, R. A. Moyer, K. H. Burrell, M. E. Fenstermacher, I. Joseph, A. W. Leonard, T. H. Osborne, G. D. Porter, M. J. Schaffer, P. B. Snyder, P. R. Thomas, J. G. Watkins, W. P. West

June 16, 2006

Nature Physics

This document was prepared as an account of work sponsored by an agency of the United States Government. Neither the United States Government nor the University of California nor any of their employees, makes any warranty, express or implied, or assumes any legal liability or responsibility for the accuracy, completeness, or usefulness of any information, apparatus, product, or process disclosed, or represents that its use would not infringe privately owned rights. Reference herein to any specific commercial product, process, or service by trade name, trademark, manufacturer, or otherwise, does not necessarily constitute or imply its endorsement, recommendation, or favoring by the United States Government or the University of California. The views and opinions of authors expressed herein do not necessarily state or reflect those of the United States Government or the University of California, and shall not be used for advertising or product endorsement purposes.

Updated October 14, 2003

Edge stability and transport control with resonant magnetic perturbations in collisionless tokamak plasmas.

Todd E. Evans,[1]* Richard A. Moyer,[2] Keith H. Burrell,[1] Max E. Fenstermacher,[3]
Ilon Joseph,[2] Anthony W. Leonard,[1] Thomas H. Osborne,[1] Gary D. Porter,[3]
Michael J. Schaffer,[1] Philip B. Snyder,[1] Paul R. Thomas,[4] Jonathan G. Watkins,[5]
and William P. West[1]

[1]General Atomics, San Diego, California, United States 92186-5608
[2]University of California, San Diego, California, United States 92093-0417
[3]Lawrence Livermore National Laboratory, Livermore, California, United States 94551-0808
Association EURATOM-CEA, CEA Cadarache, F-13108 St. Paul Lez Durance, France
[5]Sandia National Laboratories, Albuquerque, New Mexico, United States 87185
*e-mail: evans@fusion.gat.com

Abstract

A critical issue for fusion plasma research is the erosion of the first wall of the experimental device due to impulsive heating from repetitive edge magneto-hydrodynamic (MHD) instabilities known as “edge-localized modes” (ELMs). Here, we show that the addition of small resonant magnetic field perturbations completely eliminates ELMs while maintaining a steady-state high-confinement (H-mode) plasma. These perturbations induce a chaotic behaviour in the magnetic field lines, which reduces the edge pressure gradient below the ELM instability threshold. The pressure gradient reduction results from a reduction in particle content of the plasma, rather than an increase in the electron thermal transport. This is inconsistent with the predictions of stochastic electron heat transport theory. These results provide a first experimental test of stochastic transport theory in a highly rotating, hot, collisionless plasma and demonstrate a promising solution to the critical issue of controlling edge instabilities in fusion plasma devices.

Maximizing the fusion power production in toroidally symmetric magnetic confinement devices (tokamaks[1,2]) requires high-confinement (H-mode) plasma conditions that have high edge plasma pressures. A ubiquitous feature of these high edge pressure, steady state, H-mode tokamak plasmas is repetitive instabilities known as "edge-localized modes" (ELMs) which release a significant fraction of the thermal energy of the plasma to the first wall of the device. These instabilities are a class of ideal magneto-hydrodynamic (MHD) modes produced in a high pressure gradient region at the plasma edge (called the “pedestal”) where pressure gradient driven “ballooning” modes can couple to current density driven “peeling” modes[3]. While ELMs provide a natural transport process that controls the core plasma density and edge impurity ion penetration, they also represent a significant concern for burning plasma devices such as the International Tokamak Experimental Reactor (ITER)[2,4]. Based on an extensive multi-machine ELM database, it is well known that the impulsive energy released during an ELM increases with decreasing electron pedestal collisionality[5] $\nu_e^* \propto n_e^{ped} \left(T_e^{ped}\right)^{-2}$. Since burning plasmas require high electron pedestal temperatures (T_e^{ped}) at relatively high electron pedestal densities (n_e^{ped}) to achieve significant fusion power gain factors, Q ≥ 10, they must operate below $\nu_e^* = 0.1$. In this case each ELM is expected to expel up to 20% of the pedestal energy over a time interval of a few hundred μs. If allowed to reach plasma-facing wall components, energy impulses of this magnitude will cause increased erosion of plasma facing components and significantly reduce their lifetime[5,6]. Thus, controlling ELMs by replacing the energy impulses with an equivalent but more continuous transport process is a high priority issue for tokamak fusion research.

A particularly appealing ELM control approach in low ν_e^* plasmas is based on the concept of using an edge stochastic magnetic field to increase the electron thermal diffusivity χ_e across the

outer pedestal region thus reducing the electron pressure gradient ∇p_e and stabilizing peeling-ballooning (P-B) modes. Stochastic layers are created by adding small resonant magnetic perturbations (RMPs) to the equilibrium magnetic field using external coils. Experiments in high-collisionality ($\nu_e^* \geq 1.0$), low-confinement, plasmas have demonstrated that χ_e can be increased significantly across an edge stochastic layer[7-9]. Theoretically, χ_e is predicted to scale as $v_{Te} D_m$ in collisionless plasmas[10] where v_{Te} is the electron thermal velocity and D_m is a magnetic diffusion coefficient. In the quasi-linear regime D_m is proportional to the square of the normalized magnetic perturbation $\delta b_r^{(m/n)} B_\phi^{-1}$. Here, m and n are the poloidal and toroidal mode numbers respectively and B_ϕ is the toroidal magnetic field on axis (a resonance occurs when the so-called "safety factor" $q = m/n$, the ratio of the number of toroidal turns m to poloidal turns n around the torus, is a rational number[2]),.

Previous experiments in high ν_e^*, low-confinement, plasmas have demonstrated that ∇T_e is reduced across the outer region of a strong stochastic layer and increased across the inner stochastic region[7]. In addition, edge resonant magnetic perturbations with m=12-20 and n=4 were used in JFT-2M to trigger small ELMs in ELM-free H-modes[11] and to increase the frequency of small ELMs in COMPASS-D (with m=4,5 and n=1 perturbations)[12]. In DIII-D, edge-resonant perturbations with n=3 and $9 \leq m \leq 14$ were previously used to suppress large ELMs in high ν_e^* plasmas without altering the plasma confinement[13-16]. These results motivated the exploration of low-collisionality RMP pedestal and ELM control techniques in the DIII-D tokamak where high electron and ion pedestal temperatures ($T_e^{ped}, T_i^{ped} \geq 1$ keV) are regularly obtained.

Here, we report results from the first $n = 3$ edge RMP ELM control experiments in low-collisionality $0.04 \le \nu_e^* \le 0.12$, ITER relevant, DIII-D plasmas. These experiments resulted in long ELM-free H-modes, $\Delta t = 2550$ ms (17 energy confinement times), with stationary densities and radiated power levels. A detailed peeling-ballooning (P-B) analysis of these RMP assisted ELM-free H-modes shows that they operate below the peeling stability boundary and that ELMs are stabilized when RMPs reduce the edge pressure gradient ∇p, primarily through a modification in the pedestal density rather than the pedestal temperature. The observation that the RMP field causes a larger change in the edge particle balance (i.e., changes in the balance between outward particle transport and edge particle sources and sinks) rather than in the thermal transport across the pedestal is both surprising and theoretically challenging.

As in previous high ν_e^* (~ 1) RMP ELM control experiments[13-16], $n = 3$ magnetic perturbations are produced by the DIII-D I-coil located inside the vacuum vessel but outside the plasma. However, there are significant differences in the poloidal mode spectrum used in the high ν_e^* experiments versus that used in the low ν_e^* experiments discussed here. In the high ν_e^* case, the I-coil was configured to produce small magnetic islands (isolated structures on mode resonant surfaces) across the pedestal with a relatively thin stochastic boundary[15]. While this resulted in good ELM suppression with no significant change in the pedestal profiles or plasma confinement, some intermittent ELM events remained in most cases. In these high ν_e^* cases, ELMs appear to be stabilized by an increase in small transport events near the plasma edge[14]. Conversely, in the low ν_e^* experiments discussed here, the I-coil is configured to produce a highly stochastic layer covering the entire pedestal region, with relatively small remnant magnetic islands. Here, the magnitude of the RMP mode spectrum across the pedestal ($m/n =$

11/3, 12/3 and 13/3) is increased by an order of magnitude compared to the high ν_e^* low RMP case.

In both the low and high ν_e^* experiments, ELMs are only eliminated when the perturbation spectrum of the coil matches an edge resonance condition[17] determined by the helical pitch of the equilibrium magnetic field lines (the edge safety factor $q = m/n$). Figure 1 shows the ELM response to a 3 kA I-coil pulse in a lower single null poloidally diverted plasma (a plasma with a null in the poloidal magnetic field located at the bottom of the discharge[1]). In this discharge the lower DIII-D cryopump is used to pump the plasma and obtain low, ITER relevant, pedestal collisionalities. Here, 3 kA corresponds to a normalized $m/n = 11/3$ perturbation $\delta b_r^{(11/3)} B_\phi^{-1} = 2.6 \times 10^{-4}$ where $B_\phi = 2.0\,T$. Initially, while the safety factor at the 95% (q_{95}) normalized poloidal magnetic flux (ψ_N) surface $\psi_N = 0.95$ (an effective radial coordinate[18]) is above $11/3$, the RMP reduces the ELM amplitude and increases the ELM frequency from ~25 Hz to ~200 Hz. As q_{95} approaches the $11/3$ resonance condition, ELMs are completely eliminated for the remainder of the I-coil pulse. After the I-coil current is switched off, large 25-50 Hz ELMs return once the pedestal profile recovers and ∇p exceeds the P-B stability limit. Additionally, a threshold for ELM suppression is found in the neutral beam injected (NBI) heating power $P_{NBI} \geq 4.0\ MW$ (NBI powers of $10.0\ MW$ have been used with no indication of an upper power limit). There is also a threshold in the RMP amplitude as shown in Fig. 2. Here, three RMP amplitudes ranging from $\delta b_r^{(11/3)} B_\phi^{-1} = 1.7 \times 10^{-4}$ (with an I-coil current of 2 kA) to $\delta b_r^{(11/3)} B_\phi^{-1} = 3.3 \times 10^{-4}$ (with 4 kA) have been used. The ELM response at each perturbation level from high to low is shown in Figs. 2(a-c) respectively. As seen in Fig. 2(c), some ELMs remain

at 2 kA but at 3 kA [Fig. 2(b)] the ELMs are completely eliminated once q_{95} crosses 11/3. At 4 kA [Fig. 2(a)] ELMs are more strongly affected at higher q_{95} values but not completely eliminated until reaching $q_{95} = 11/3$. This indicates a slight increase in the width of the safety factor resonance with increasing perturbation amplitude.

During the initial off-resonance phase of the RMP pulse ($q_{95} > 11/3$) an increase in energy transport caused by small, high frequency, ELMs commands the normalized plasma pressure (β_N) feedback system to increase the NBI power by ~15-20%. Once the q_{95} resonance condition is satisfied, these small ELMs disappear, leaving the plasma in a very quiet state (Fig. 3a), and the pedestal density n_e^{ped} begins to fall while T_e^{ped} continues to slowly increase (Fig. 3b). The electron pedestal pressure (Fig. 3b) drops initially following the suppression of the small ELMs and remains relatively constant throughout the remainder of the RMP pulse. The thermal energy content of the plasma (Fig. 3c) increases slowly during the rapid ELMing phase due to the increased NBI power and reaches a relatively stationary level once the small ELMs disappear. In addition, the total power radiated from the plasma P_{rad_tot} remains constant throughout the ELM-free phase (Fig. 3d). During the rapid ELMing phase at 1.9 s, the electron density on axis is $n_{eo} = 5.2 \times 10^{19} \mathrm{m}^{-3}$ and the central electron temperature is $T_{eo} = 3.7\ keV$. At 3.5 s with no ELMs $n_{eo} = 3.8 \times 10^{19} \mathrm{m}^{-3}$ and $T_{eo} = 4.0\ keV$. This change in n_{eo} along with the entire density profile is indicative of a dramatic change in the particle balance once the ELMs are suppressed. At the same time global energy confinement time (τ_E) shows a modest increase from 130 ms at 1.9 s to 147 ms at 3.5 s. While the ELM-free properties of these discharges are similar in some respects to Quiescent H-modes in DIII-D[19] they do not have edge harmonic oscillations[19], which are

thought to be responsible for the particle transport out of the pedestal in the Quiescent H-mode case.

Changes in the edge plasma profiles during the RMP ELM-free phase are indicative of a significant alteration in the particle balance with a relatively small change in the energy transport and are qualitatively inconsistent with stochastic transport theory[10]. Figure 4 shows how the edge T_e, T_i and n_e profiles change, when averaged over a 600 ms time window, during the ELM-free phase with I-coil currents of 2 and 3 kA compared to an equivalent window during an ELMing phase with no I-coil current just before the onset of an ELM (the 0 kA case). The T_e profile [Fig. 4(a)] appears to decrease from $\psi_N = 0.85$ out to just beyond $\psi_N = 0.93$ and increases out to the top of the pedestal with the RMP. Comparing the 2 kA, marginally stable, case with the 0 kA case, we see that the electron pedestal temperature gradients ∇T_e^{ped} are a good match to within the experimental uncertainty. As the coil current is increased to 3 kA we see the formation of a higher/narrower pedestal structure compared to the profile (*i.e.*, an increase in ∇T_e^{ped} and a corresponding decrease in χ_e in the region $0.99 \le \psi_N \le 1.0$). This is inconsistent with the expectation from stochastic transport theory[10] that χ_e should increase significantly across a broad ($\Delta\psi_N \approx 0.1$) stochastic layer induced by the RMP. No profiles have been found during these experiments with the expected ∇T_e^{ped} decrease and a corresponding increase in χ_e over the last 1-2% in ψ_N. In contrast, we note that in the region near the top of the pedestal the profile is quite flat compared to the unperturbed case (particularly with 3 kA). This may indicate that quasi-linear diffusion theory is qualitatively more applicable in that region of the plasma than in the steep pedestal gradient region. Additionally, as shown in Fig. 4(b), the T_i profile increases

across the entire plasma edge and ∇T_i^{ped} increases just inside the unperturbed separatrix (the unperturbed separatrix is the 2D poloidal boundary that separates closed magnetic field lines inside from field lines that hit plasma-facing components outside). These changes in the pedestal T_e and T_i profiles are in sharp contrast to the n_e profile behaviour shown in Fig. 4(c). Here, the density at the unperturbed separatrix location $n_{e_sep}(\psi_N = 1.0)$ decreases significantly with the I-coil on compared to the zero current case and the density gradient ∇n_e is reduced near $\psi_N = 1.0$ along with the radial extent of ∇n_e (i.e., the "pedestal" is narrower).

In these experiments we consistently find that, within experimental uncertainty, RMP ELM-free discharges are stable to peeling-ballooning modes, while ELMing discharges become unstable to peeling-ballooning modes just before an ELM occurs. Profile data such as those in Fig. 4 are used in the ELITE code[3,20] to evaluate the peeling-ballooning mode stability for a rather extensive collection of ELMing and RMP assisted ELM-free discharges. Using accurate global reconstructions of the observed equilibria, and non-local stability calculations with full plasma profiles along with a broad range of unstable mode numbers (n=5-30). We represent these non-local stability results in a simplified manner in Fig. 5. Here, the global experimental profiles are characterized by representative local values. Figure 5 shows that in RMP assisted ELM-free discharges (green ellipses) the normalized growth rate resides inside the stable region when the error bars on the data are taken into consideration. On the other hand, discharges with ELMs (magenta diamonds) consistently reside outside the stability boundary in Fig. 5. This figure also demonstrates that RMP assisted ELM-free discharges exist in the peeling-ballooning stable region (and can be deeply stable *e.g.*, with increasing RMP current as indicated by the red

I-coil currents in Fig. 5), while ELMing discharges become unstable to peeling-ballooning modes before ELMs are observed.

Although the precise amplitude of the RMP perturbations on resonant magnetic surfaces across the pedestal is difficult to establish in a rotating, high pressure plasma (due to uncertainties such as shielding or amplification produced by the plasma response to the perturbation), an estimate of the vacuum magnetic field perturbation spectrum $\delta b_r^{(m/n)}$ is useful for interpreting changes observed in the edge transport when the RMP is applied. A contour plot of a typical poloidal mode spectrum for the $n = 3$ components of $\delta b_r^{(m/n)}$ used in these experiments is shown in Fig. 6. The dashed black curve shows the location, along the contours, of the mode resonant surfaces. Discrete harmonic resonances are indicated by black dots satisfying the condition $m = nq(\psi_N)$. We note that for the I-coil configuration used in these low ν_e^* discharges the pedestal resonances, $11 \le m \le 13$, all have roughly equal amplitudes near the maximum value of the spectrum (~4.2 G).

Using the data from Fig. 6 we estimate the stochastic magnetic field diffusivity based on quasi-linear theory[10] as $D_{m,n}^{ql}\,(\mathrm{m}) = \pi R_0 \sum_{m=11-13}^{n=3} q_{m,n} (\delta b_r^{(m/n)} B_T^{-1})^2\,(\mathrm{m}) = 3.5 \times 10^{-6}\,(\mathrm{m})$. Numerical calculations of the stochastic magnetic field diffusivity yield $D_m = 3.9 \times 10^{-6}\,(\mathrm{m}^2/\mathrm{s})$ for the same conditions as above[21]. Thus, for $T_e^{ped} = 1.1\,keV$, $\mathrm{v}_{Te} = 1.4 \times 10^7\,(\mathrm{m/s})$ the cylindrical quasi-linear thermal diffusivity is $\chi_{m,n}^{ql}\,(\mathrm{m}^2/\mathrm{s}) = \mathrm{v}_{Te} D_{m,n}^{ql}\,(\mathrm{m}^2/\mathrm{s}) = 49\,(\mathrm{m}^2/\mathrm{s})$. Using $D_{m,n}^{ql}$ and the ion sound speed $\mathrm{c}_s\,(\mathrm{m/s}) = \sqrt{(T_e + \gamma_i T_i)/m_i}\,(\mathrm{m/s}) = 5.5 \times 10^5\,(\mathrm{m/s})$ where $T_i^{ped} = 1.8\,keV$, $\gamma_i = 3$ and m_i is the mass of the deuterium ions used in these plasmas, the stochastic particle diffusivity across the pedestal is $1.9\,(\mathrm{m}^2/\mathrm{s})$. Then, using the electron heat flux crossing $\psi_N = 0.95$ ($q_e = P_e/A_{\psi 95}$ where $P_e = 2.4\,MW$

is the heating power absorbed by the electrons and $A_{\psi 95} = 49.3\,\mathrm{m}^2$ is the surface area at $\psi_N = 0.95$) we find $\chi_e^{\exp} = q_e / n_e \nabla T_e = 2.8\left(\mathrm{m}^2/\mathrm{s}\right)$ based on the 3 kA T_e profile shown in Fig. 4a and n_e from Fig. 4c. In the high-gradient region where $\psi_N = 0.985$, we find $\chi_e^{\exp} = 0.1\left(\mathrm{m}^2/\mathrm{s}\right)$. Thus, there is a significant difference between the quasi-linear and experimental thermal diffusivity in the high-gradient region, where $\chi_{m,n}^{ql} / \chi_e^{\exp} \sim 500$, while just inside the top of the pedestal at $\psi_N = 0.95$ this difference is reduced to $\chi_{m,n}^{ql} / \chi_e^{\exp} \sim 18$ which is a rather modest difference given the uncertainties in the experimental and quasi-linear estimates. A similar estimate of the thermal diffusivity with no I-coil current gives $0.8\left(\mathrm{m}^2/\mathrm{s}\right)$ at $\psi_N = 0.95$ and transport modelling using χ_e as a free parameter in the 2D UEDGE fluid code[22] results in a reasonably good match with the black (0 kA) T_e profile shown in Fig. 4a inside $\psi_N = 0.95$ when $\chi_e = 1.4\left(\mathrm{m}^2/\mathrm{s}\right)$. Although estimates of the particle diffusivity ($D_{\perp e}$) are more difficult to assess because of uncertainties in local sources and sinks, UEDGE modelling, with zero I-coil current, gives a reasonable match to the experimental data with $D_{\perp e} = 0.1\left(\mathrm{m}^2/\mathrm{s}\right)$. This increases to $D_{\perp e} = 0.2\left(\mathrm{m}^2/\mathrm{s}\right)$ with an I-coil current of 3 kA. These results indicate that in the pedestal χ_e is several orders of magnitude smaller than expected based on quasi-linear theory and appears to decrease slightly during the 3 kA RMP pulse. Thus, stochastic transport theory alone cannot explain the experimental results.

The experimental data is also inconsistent with predictions of the RMP screening level due to the toroidal rotation of the plasma. During the initial part of the RMP pulse the pedestal safety factor profile is well above the optimal value required for a strong stochastic layer, *i.e.*, the resonance curve in Fig. 6 lies to the right of the spectral peak reducing the amplitude of the resonant $\delta b_r^{(m/n)}$ components. Then, as the pedestal safety factor profile approaches the optimal

resonant condition the small high frequency ELMs are eliminated and the increasing stochastic transport compensates the loss of ELM-driven transport. Simultaneously, the average toroidal rotation of the edge plasma Ω_ϕ just inside the unperturbed separatrix increases by ~3 kHz. Based on magnetic shielding theory[23], this change in Ω_ϕ should reduce $\delta b_r^{(m/n)} B_\phi^{-1}$ by about a factor of 100. A reduction of this magnitude would imply that the RMP fields are unable to create a stochastic layer because the widths of the resulting magnetic islands should be significantly smaller than their separation and they will not overlap. Thus, rotational shielding, in its present form, contradicts several experimental observation: the dramatic reduction in n_e, the increase in Ω_ϕ across the pedestal and the increase in χ_e at $\psi_N \leq 0.95$ when q_{95} crosses 11/3 as well as the resonant character of the ELM suppression.

Resonant magnetic perturbations (RMPs), produced by the DIII-D I-coil configured for strongly resonant $n = 3$ operations, have been used to achieve stationary ELM-free H-modes at ITER relevant collisionalities. During the ELM-free phase of these discharges the density and radiated power remain stationary for long periods of time (up to 2550 ms or about 17 energy confinement times). Comparisons with peeling-ballooning mode stability theory indicates that the ELMs are eliminated by an RMP-induced reduction in the pedestal pressure gradient. This reduction in the pedestal pressure gradient pushes the operating point of the discharge below the ELM instability boundary. The reduced pedestal pressure is brought about by a reduction in the pedestal particle content rather than an increase in the pedestal thermal diffusivity. We find that stochastic diffusion theory over estimates the electron thermal transport determined from the experimental data. In addition, unambiguous signatures of a resonant behaviour in the perturbing magnetic field are observed in the experiments while estimates of resonant magnetic field shielding factors, due to the flow of a rotating plasma through a static perturbing field, suggest

that strong magnetic field resonances should not occur and that a stochastic layer should not form. Thus, the experimental results are both surprising and theoretically challenging since they indicate that stochastic transport theory and RMP shielding theory are incomplete when applied to highly rotating collisionless pedestal plasmas. In addition, these experiments indicate that externally applied $n = 3$ resonant magnetic perturbations may be a promising option for controlling ELMs and pedestal transport in future tokamak fusion plasmas.

ACKNOWLEDGMENTS

We would like to thank R.J. La Haye for pointing out that magnetic shielding due to edge plasma rotation may be a significant effect in these experiments. This work was supported by the U.S. Department of Energy under DE-FC02-04ER54698,W-7405-ENG-48 (LLNL), and DE-FG02-04ER54758.

REFERENCES

1. Callen, J. D., Carreras, B. A., & Stambaugh, R. D. Stability and transport processes in tokamak plasmas. Phys. Today 45 34-42 (1992).

2. Wesson, J. *Tokamaks*, 711-717 Ch. 13 (Oxford Univ. Press, Oxford, 3rd Ed. 2004).

3. Snyder, P. B. *et al*. Edge localized modes and the pedestal: A model based on coupled peeling-ballooning modes. *Phys. Plasmas* **9**, 2037-2043 (2002).

4. ITER Website http://www.iter.org.

5. Loarte, A. *et al*. Characteristics of type I ELM energy and particle losses in existing devices and their extrapolation to ITER. *Plasma Phys. Control. Fusion*, **45**, 1549-1569 (2003).

6. Loarte, A. *et al*. ELM energy and particle losses and their extrapolation to burning plasma experiments. *J. Nucl. Mater.* **313-316**, 962-966 (2003).

7. Evans, T. E. *et al*. Experiments to test an intra-island scoop limiter on TEXT. *J. Nucl. Mater*. **145-146**, 812-815 (1987).

8. Ghendrih, Ph., Grosman, A. & Caps, H. Theoretical and experimental investigations of stochastic boundaries in tokamaks. Plasma Phys. Control. Fusion **38** 1653-1724 (1996).

9. Jakubowski, M. W. et al. Change of the magnetic-field topology by an ergodic divertor and the effect on the plasma structure and transport. Phys. Rev. Lett. **96**, 035004-1 (2006).

10. Rechester, A. B. & Rosenbluth, M. N. Electron heat transport in a tokamak with destroyed magnetic surfaces. *Phys. Rev. Lett.* **40**, 38-41 (1978).

11. Mori, M. et al. Plasma improvement with ergodic magnetic fields in JFT-2M. Proc. International Conf. on Control. Fusion and Plasma Phys., Würzburg, Austria (1992) **2**, 567-573 (1992).

12. Fielding, S. J. et al. ELM control in COMPASS-D. Proc. of 28th EPS Conference on Contr. Fusion and Plasma Phys., Funchal, Portugal, 18-22 June 2001. ECA **25A**, 1825-1828 (2001).

13. Evans, T. E. *et al.* Suppression of Large edge-localized modes in high-confinement DIII-D plasmas with a stochastic magnetic boundary. *Phys. Rev. Lett.* **92**, 235003-1 (2004).

14. Moyer, R. A. *et al.* Edge localized mode control with an edge resonant magnetic perturbation. *Phys. Plasmas* **12**, 056119-056119-11 (2005).

15. Evans, T. E. *et al.* Suppression of large edge localized modes with edge resonant magnetic fields in high confinement DIII-D plasmas. *Nucl. Fusion* **45**, 595-607 (2005).

16. Evans, T. E. *et al.* Suppression of large edge localized modes in high confinement DIII-D plasmas with a stochastic magnetic boundary. *J. Nucl. Mater.* **337-339**, 691-696 (2005).

17. Burrell, K. H. *et al.* ELM suppression in low edge collisionality H-mode discharges using n=3 magnetic perturbations. *Plasma Phys. Control. Fusion* **47,** B37-B52 (2005).

18. D'haeseleer, W. D., Hitchon, W. N. G., Callen, J. D., & Shohet, J. L. *Flux Coordinates and Magnetic Field Structure,* (Springer-Verlag, Berlin, 1991).

19. Burrell, K. H. *et al.* Advances in understanding quiescent H-mode plasmas in DIII-D. *Phys. Plasmas* **12**, 056121-056121-10 (2005).

20. Wilson, H. R., Snyder, P. B., Huysmans, G. T. A. & Miller, R. L. Numerical studies of edge localized instabilities in tokamaks. *Phys. Plasmas* **9**, 1277-1286 (2002).

21. Evans, T. E. et al. The physics of edge resonant magnetic perturbation in hot tokamak plasmas. Phys. Plasmas **13**, (to appear May 2006).

22. Porter, G. D. et al. Characterization of the separatrix plasma parameters in DIII-D. Phys. Plasmas **5**, 1410-1422 (1998).

23. Fitzpatrick, R. Bifurcated states of a rotating tokamak plasma in the presence of a static error-field. *Phys. Plasmas* **5**, 3325-3341 (1998).

FIGURE CAPTIONS

Figure 1 ELM response to an applied magnetic perturbation: Lower divertor D_α intensity, q_{95} safety factor at the 95% normalized poloidal flux surface evolution, and applied I-coil current in DIII-D discharge #122336.

Figure 2 Changes in the ELM response with increasing magnetic perturbation levels: Divertor D_α emission (particle recycling light) with I-coil currents of: (a) 4 kA, (c) 3 kA and (d) 2 kA. In these discharges, the I-coil current typically remains constant until 5 s when it is switched off due to hardware limitations on the length of the plasma discharge.

Figure 3 The value of the safety factor at the 95% magnetic flux surface (q_{95}) influences the response of the ELMs to the RMP: (a) ELMs are seen as spikes in the Divertor D_α emission (particle recycling light) which disappear as q_{95} crosses 11/3, (b) the electron pedestal pressure, density and temperature, (c) the energy content of the plasma (stored energy) and the RMP current amplitude, and (d) the injected neutral beam heating power (NBI Power) and total power radiated from the plasma.

Figure 4 Changes in the edge plasma profiles with various magnetic perturbation levels: Edge (a) electron and (b) ion temperature and (c) electron density profiles with no I-coil (black, #122336), 2 kA (red, #122344) and 3 kA (green, #122337) versus normalized poloidal magnetic flux (ψ_N). The edge pedestal beyond $\psi_N > 0.95$ is most clearly seen in the T_e profile for the 3 kA case. The solid curves are fits to the data points showing the average profiles over the data window. Error bars representing uncertainties due to photon statistics (statistical fluctuations in the signal and observed background noise) in the Thomson scattering measurements are shown on the individual data points.

Figure 5 ELM stability diagram: Normalized peeling-ballooning mode growth rates $\gamma_N \equiv \gamma/0.5\omega_{*e}$ (where γ is the peeling-ballooning growth rate and ω_{*e} is the electron drift frequency across the magnetic field referred to as the diamagnetic drift frequency) are shown for 6 ELMing (magenta diamonds) just before the onset of an ELM and 14 RMP-induced ELM-fee (green ellipses) cases. Here, γ_N is plotted as a function of the maximum value of the normalized pedestal pressure gradient $\alpha = -\left(2\mu_o/(2\pi)^2\right)\partial V/\partial\psi\left(V/2\pi^2 R_o\right)\partial p/\partial\psi$ (where V is the plasma volume, p is the pressure, ψ is the poloidal magnetic flux and R_o is the major radius of the plasma) and a characteristic pedestal current density j_N^{ped} which is taken to be the peak value of the parallel current in the pedestal region normalized by the average parallel current in the pedestal. These points are a local representation of the fastest growing mode based on the entire pedestal profile. Representative error bars are shown on the data point at $\alpha = 3.4$ and $j_N^{ped} = 0.53$. The colour bar on the right shows the value of γ_N for each experimental profile modelled with the stability code.

Figure 6 Contour plot of the magnetic perturbation spectrum: The Fourier amplitude of the $n = 3$ magnetic field from a 2 kA I-coil current in plasma discharge 122344 is shown as a function of poloidal mode number and normalized poloidal flux ψ_N and includes perturbations from all measured sources of field-errors in DIII-D. White contour lines are drawn at each 10% change in amplitude and $m = nq$ (ψ_N) resonances (black dots) lie along a ridge in the contours of the perturbing field. The colour bar on the right shows the amplitude scale in Gauss. Red is high and black is low.

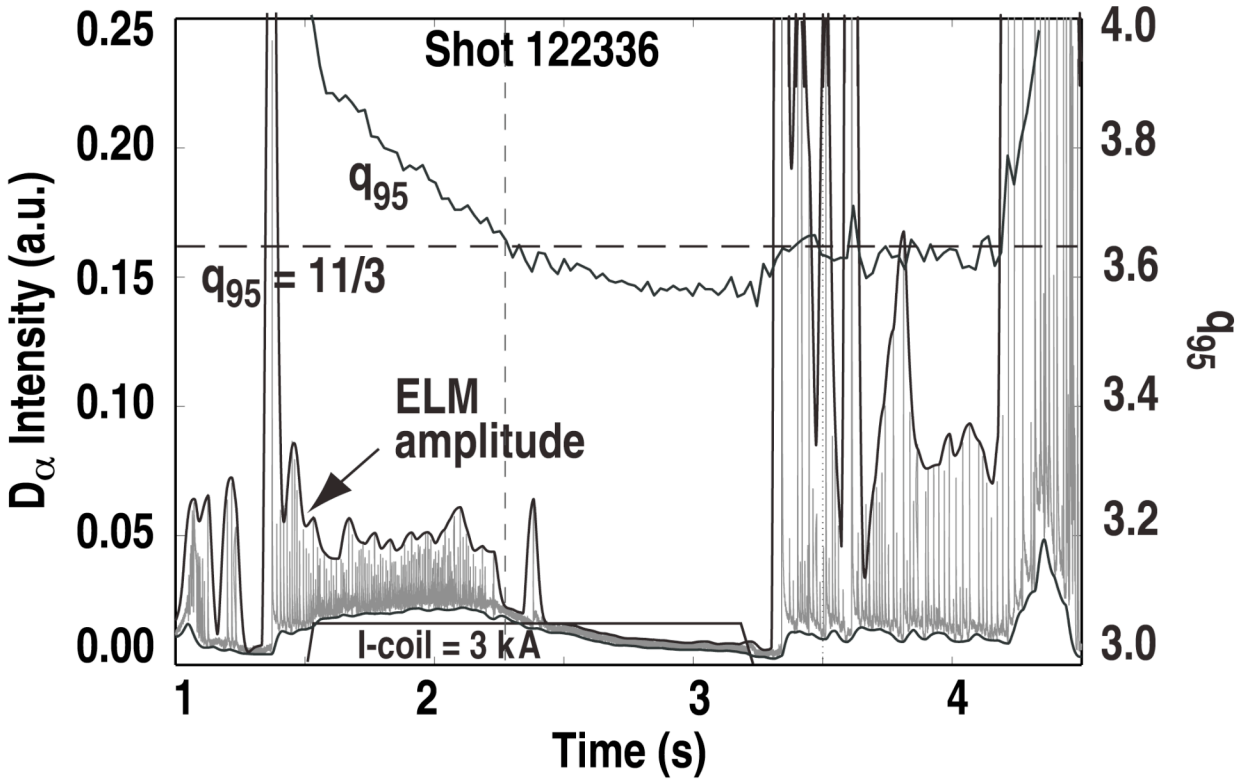
Shot 122336
q_{95}
q_{95} = 11/3
ELM
amplitude
I-coil = 3 kA
D_α Intensity (a.u.)
q_{95}
Time (s)
0.25
0.20
0.15
0.10
0.05
0.00
4.0
3.8
3.6
3.4
3.2
3.0
1
2
3
4

Figure 1

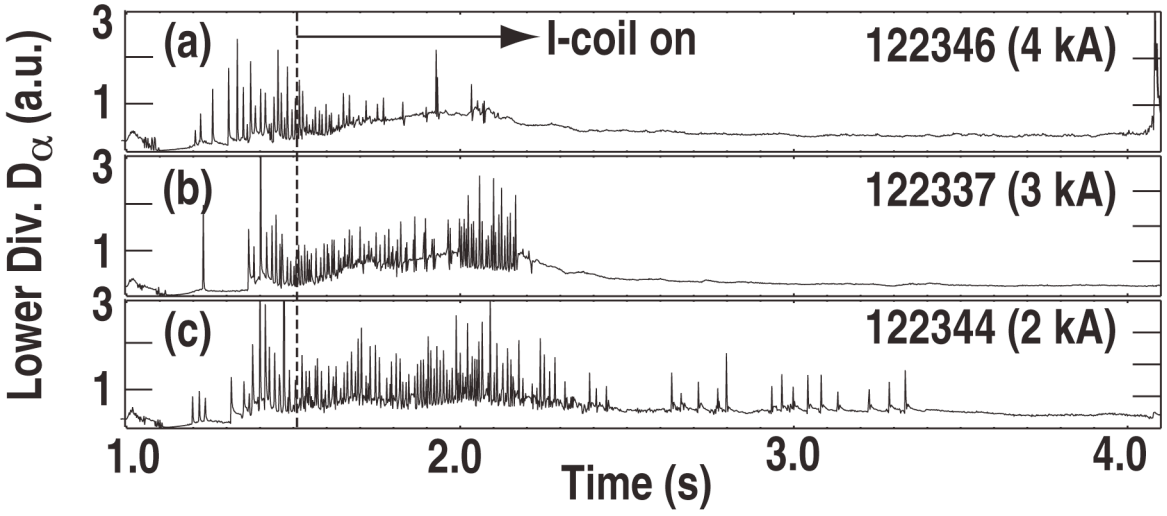
Lower Div. D_α (a.u.)
3
1
(a)
I-coil on
122346 (4 kA)
3
1
(b)
122337 (3 kA)
3
1
(c)
122344 (2 kA)
1.0
2.0
3.0
4.0
Time (s)

Figure 2

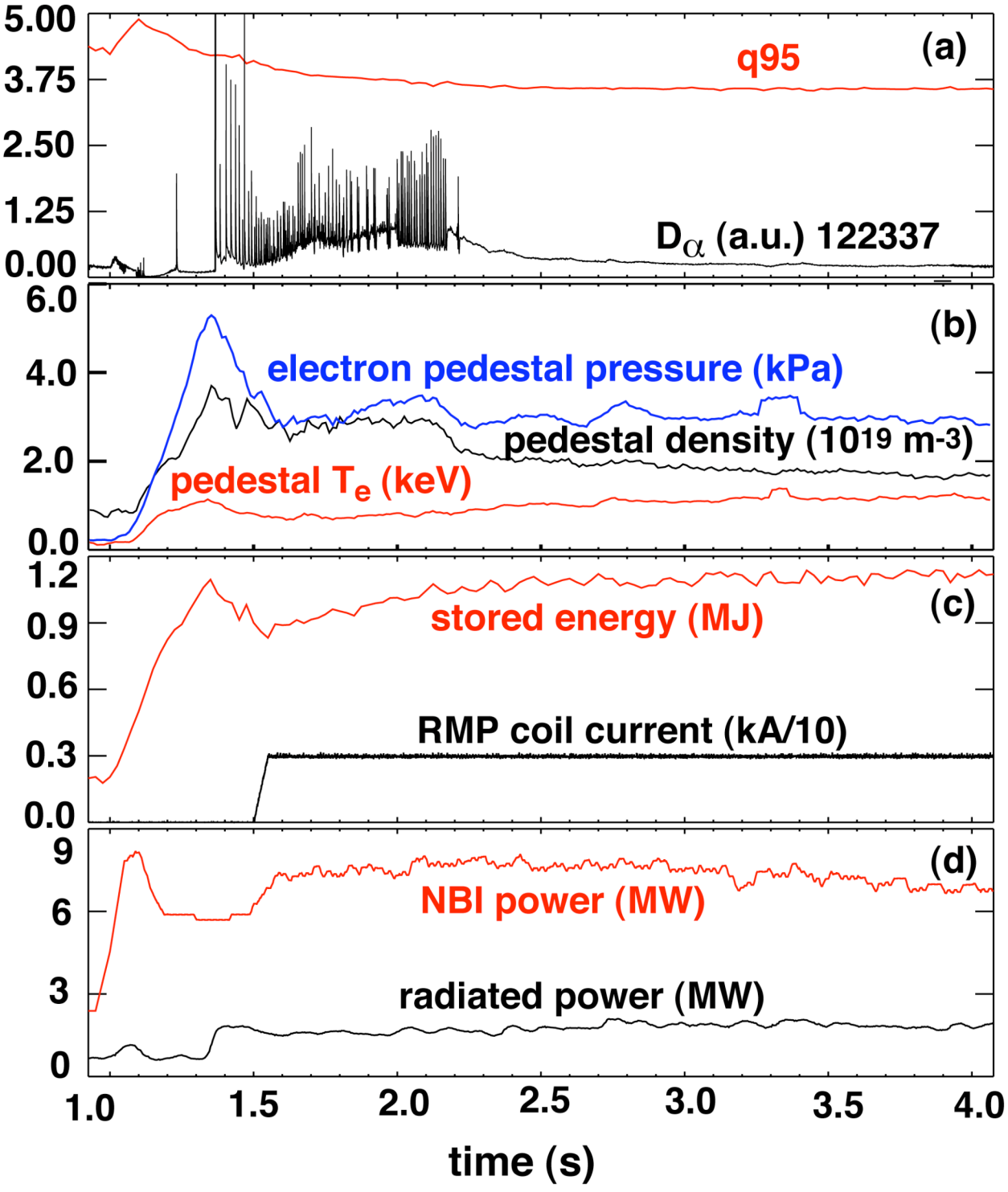
5.00
3.75
2.50
1.25
0.00
q95
(a)
D_α (a.u.) 122337
6.0
4.0
2.0
0.0
(b)
electron pedestal pressure (kPa)
pedestal density (10^{19} m^{-3})
pedestal T_e (keV)
1.2
0.9
0.6
0.3
0.0
(c)
stored energy (MJ)
RMP coil current (kA/10)
9
6
3
0
(d)
NBI power (MW)
radiated power (MW)
1.0
1.5
2.0
2.5
3.0
3.5
4.0
time (s)

Figure 3

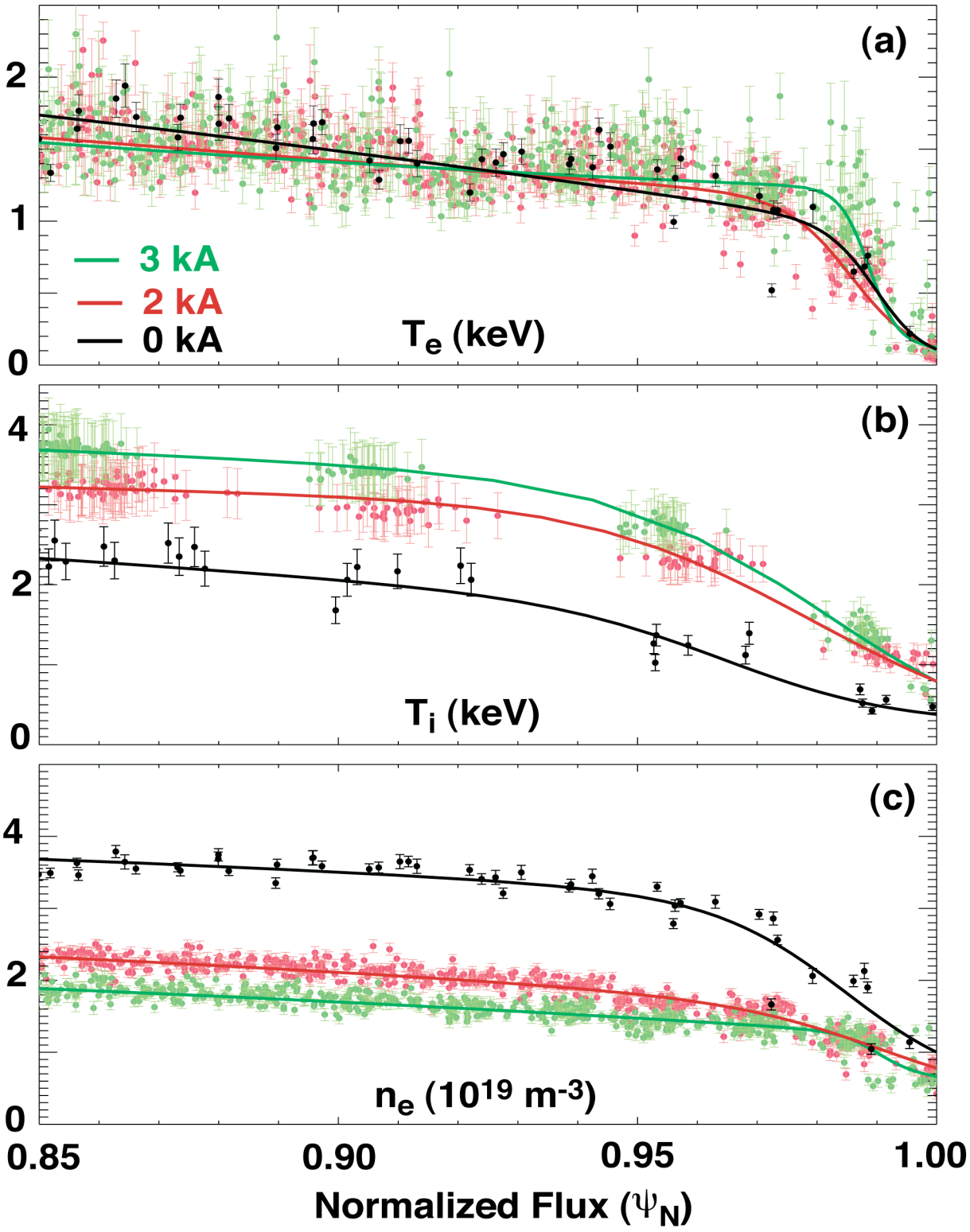
(a)
3 kA
2 kA
0 kA
T_e (keV)
(b)
T_i (keV)
(c)
n_e (10^{19} m^{-3})
0.85
0.90
0.95
1.00
Normalized Flux (Ψ_N)

Figure 4

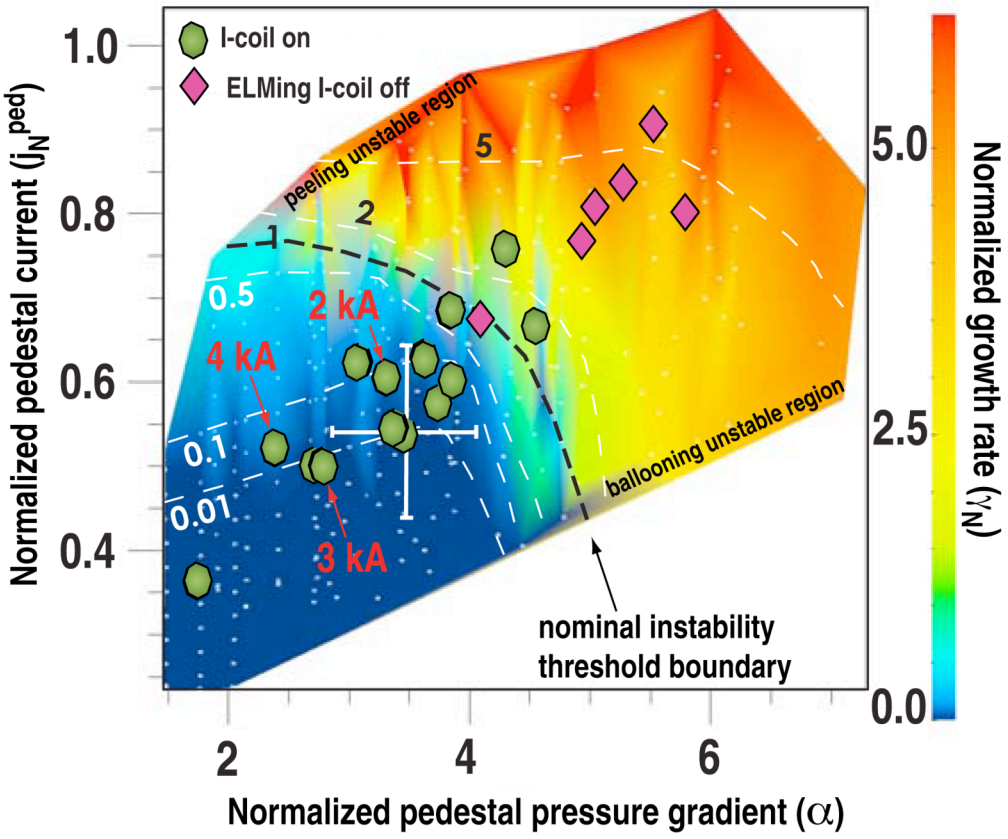
I-coil on
ELMing I-coil off
peeling unstable region
ballooning unstable region
nominal instability
threshold boundary
5
2
1
0.5
0.1
0.01
2 kA
4 kA
3 kA
1.0
0.8
0.6
0.4
Normalized pedestal current (j_N^{ped})
2
4
6
Normalized pedestal pressure gradient (α)
5.0
2.5
0.0
Normalized growth rate (γ_N)

Figure 5

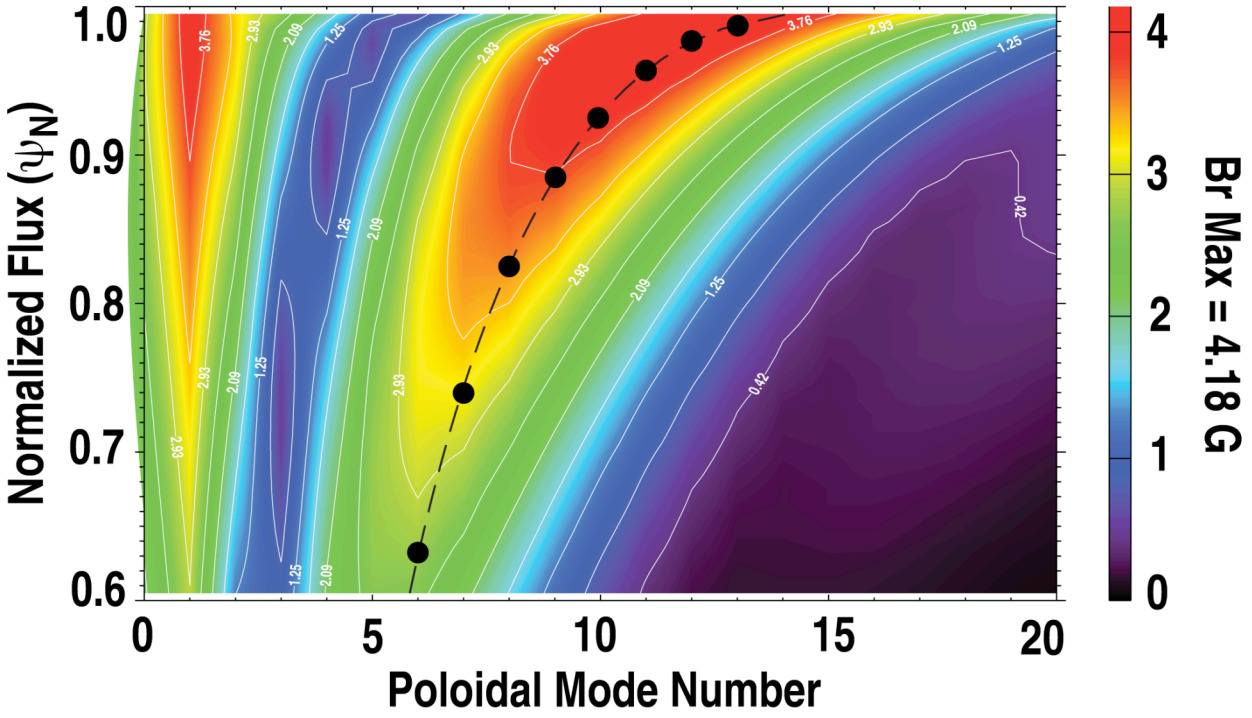
Normalized Flux (ψ_N)
1.0
0.9
0.8
0.7
0.6
0
5
10
15
20
Poloidal Mode Number
Br Max = 4.18 G
4
3
2
1
0
3.76
2.93
2.09
1.25
0.42

Figure 6